Polarization dependence of phonon and electronic Raman intensities in $PrVO_4$ and $NdVO_4$

An-Dien Nguyen, Keith Murdoch, and Norman Edelstein
Chemical Sciences Division, Lawrence Berkeley National Laboratory, Berkeley, California 94720
and Department of Physics, University of California, Berkeley, California 94720

L. A. Boatner and M. M. Abraham
Solid State Division, Oak Ridge National Laboratory, Oak Ridge, Tennessee 37831
(Received 21 January 1997)

The polarization behavior of the phonon and electronic Raman intensities in $PrVO_4$ and $NdVO_4$ has been measured. These experimental intensities are compared with the intensities predicted by a polarization-dependent intensity theory. Good agreement was found between theory and experiment. The fitted values of the ratio F_1/F_2 for $PrVO_4$ and $NdVO_4$ were found to be 1.0 and 0.48, respectively. The relative values of the α_q^t parameters obtained from the fit were compared with theoretical values which were derived using both second- and third-order theory, where the latter included the spin-orbit interaction. Axe's second-order theory was found to adequately explain the relative intensities of electronic Raman transitions in $PrVO_4$ and $NdVO_4$. [S0163-1829(97)06037-2]

I. INTRODUCTION

Raman scattering experiments between electronic states of rare-earth (RE) ions in a crystal were reported by Hougen and Singh[1] in 1963. The quantitative electronic Raman theory incorporating Axe's two-photon theory[2] for RE ions in crystalline hosts was subsequently developed by Koningstein and Mortensen.[3,4] Two-photon absorption (TPA) is a process in which two photons are simultaneously absorbed. When an incident photon is instantaneously absorbed by the atom and the second photon scattered, the process is called electronic Raman scattering (ERS). Both TPA and ERS have been used complementarily to locate and determine the symmetries of crystal-field levels in various materials. While TPA has been used to probe energy levels in the uv region, ERS has provided information about the low-lying levels.[5] With the aid of Axe's theory, intensity calculations for transitions between crystal-field levels of the $4f^N$ ground configuration of RE materials have been possible and become a fruitful research area of quantitative two-photon spectroscopy.[6–8] Axe's theory, however, was inadequate to explain TPA intensities of the Gd^{3+} ion in Gd^{3+}:LaF_3, $GdCl_3$, and $Gd(OH)_3$ and of the Eu^{2+} ion in Eu^{2+}:CaF_2 and Eu^{2+}:SrF_2.[9–13] One reason why discrepancies exist between theory and experiment in the materials reported above is that the leading matrix element of the two-photon second-order tensor operating between the initial and final $4f^N$ states is exceedingly small for a $4f^7$ system, such as Gd^{3+} and Eu^{2+}. This lack of agreement with theory prompted several workers to extend the second-order theory of Axe to include higher-order terms in the perturbation expansion. For example, Judd and Pooler[11] developed a third-order perturbation theory, which includes the spin-orbit interaction, to account for the ${}^8S_{7/2} \rightarrow {}^6P_J$ transition intensities of Gd^{3+} ions. Downer and Bivas[10] later expanded Axe's theory to the fourth order to include both the spin-orbit and crystal-field interactions to explain the observed ${}^8S_{7/2} \rightarrow {}^6P_J, {}^6D_J$ transition intensities of Gd^{3+} ions in Gd^{3+}:LaF_3. More recently, Smentek-Mielczarek[14] included correlation contributions in the third-order scheme.

Another test of Axe's theory involves comparison between the observed and calculated intensities of the electronic Raman transitions in RE doped crystals. Following Koningstein and Mortensen's observation[15,16] that ERS spectra display asymmetric features (e.g., $I_{XZ} \neq I_{ZY}$, where the subscripts indicate the respective polarizations of the scattered and incident photons measured in the crystal axis system[17]), Becker *et al.*[6] showed that the ratio I_{XZ}/I_{ZY} may provide a sensitive test for the second-order theory. This intensity ratio is directly related to the ratio F_1/F_2 (defined below), which in turn depends on the properties of the particular RE ion being considered. Nevertheless, Becker's extensive study of ERS in RE phosphate crystals yielded poor agreement between the observed and predicted asymmetry ratios.[6,7] This inadequacy of the second-order theory motivated further theoretical investigations in the third-order regime by Smentek-Mielczarek.[18] Even with the extension to the third-order theory, only moderate agreement with observed data was found.

Recently the two-photon theory has been expanded and expressions derived for the polarization-dependent intensity (PDI) behavior of the TPA transitions.[19,20] The results can also be applied to phonon scattering and to ERS. A tabulation of the two-photon PDI functions for the 32 crystallographic point groups has been given. PDI functions for two-photon transition intensities had previously been reported by Bader and Gold.[21] However, Bader and Gold's PDI expressions contain a number of parameters which cannot be predicted by their theory. For a particular symmetry, the new theory gives PDI functions that can be tested. If Axe's theory is utilized, the two parameters F_1 and F_2 can be calculated and compared with the values obtained from the empirical PDI behavior.

A more general method to obtain a fitted value for the ratio F_1/F_2 is possible. Previously this ratio was extracted from only two data points, namely I_{XZ} (or I_{YZ} for D_{2d} sym-

metry) and I_{ZX} (or I_{ZY}).[6–8] The new method, however, allows the extraction of the ratio from an unlimited number of data points associated with the intensities measured at arbitrary polarization angles with respect to the crystal axis system.

In this paper the PDI behavior of phonon and electronic Raman transitions in the ground multiplets of Pr^{3+} ions in $PrVO_4$ and of Nd^{3+} ions in $NdVO_4$ is reported and compared with that predicted using the formalism developed in Refs. 19 and 20. The fitted values for the ratio of F_1/F_2 for Pr^{3+} and Nd^{3+} are given and compared with the values predicted using Axe's theory, which takes into account the $4f^{N-1}5d$ orbital configuration. The relative intensities of the electronic Raman transitions originating in the ground multiplets of Pr^{3+} and Nd^{3+} ions are also compared with theory.

II. EXPERIMENT

The samples used were single crystals grown at the Oak Ridge National Laboratory. The single crystals have typical dimensions of 1 mm×1 mm×6 mm. The crystals LVO_4 (L = La-Lu) have D_{4h} space group symmetry, with the trivalent L ion at a D_{2d} symmetry site. In the x,y,z molecular axis system, the z axis of this site is parallel to the crystallographic c axis, which is the Z axis in the X,Y,Z crystal axis system. The x and y axes, which are the twofold C_2 axes, are rotated about the z axis by 45° relative to the X and Y crystallographic axes.[22,23]

The excitation beam for the ERS experiment was produced by a Coherent Innova model 306 cw argon-ion laser. All the polarization measurements reported for $PrVO_4$ were obtained using the 514 nm laser line, which was the only nonresonant excitation wavelength. The 488 nm excitation line was used for intensity measurements in $NdVO_4$. The vertically polarized output of the laser was passed through a Spectra Physics model 310-21 polarization rotator, which could vary the polarization of the beam arbitrarily over 360°. An achromatic doublet lens with a focal length of 15 cm was used to focus the beam onto the crystal. The power was adjusted so that a 50 mW beam was incident on the crystal, usually with a beam diameter on the order of 200 μm. The sample was mounted inside an Oxford Instruments model CF1204 cryostat. The crystal was cooled to 4.2 K in all ERS scans to avoid temperature broadening. The sample temperature was monitored by an Oxford Instruments model ITCV4 temperature controller. The scattered light was collected at an angle 90°. The collection optics used included a Nikon camera lens with a focal length of 5 cm and an achromatic doublet with a focal length of 33 cm. A polarization scrambler and a Dove prism were placed after a polarization analyzer. The scattering signal was dispersed by a Spex 1403 double monochromator and detected by a Hamamatsu R375 photomultiplier tube. Slit widths were set at 250 μm in all scans, which allow a spectral bandpass of approximately 2.5 cm^{-1}. The signal was then amplified by a Stanford Research model SR450 Preamplifier and measured by a Stanford Research model SR400 photon counter interfaced to a PC computer. Phonon spectra were taken at both room temperature and low temperature to ensure proper alignment of the crystal. Polarization leakage was negligible for all phonon symmetries.

The PDI spectra were obtained by the following procedure. A total of 45 scans were recorded, each corresponding to a polarization state $(\theta_1,\varphi_1,\theta_2,\varphi_2)$, where θ represents the polar angle of the polarization vector measured from the z axis in the molecular coordinate system, φ the azimuth angle measured from the x axis in the xy plane, 1 the incident photon, and 2 the scattered photon. The incident polarization angle θ_1 was initially set to 0°, while the scattered polarization angle θ_2 was incremented for each successive scan by 22.5°, from 0 to 180°. Then θ_1 was incremented to 22.5°, and the process repeated until θ_1 reached 90°. For calibration purposes, a pair of electronic Raman and phonon scattering spectra with similar PDI curves were taken concurrently for each polarization state of the incident and scattered light. To calibrate the ERS intensities, the ratio of the predicted to the measured phonon intensity for each polarization state was used to scale the ERS intensity corresponding to that state. The detailed calibration procedure can be found in Ref. 19.

The observed linewidths were fitted using the computer program GRAMS. The electronic Raman transitions were fitted to Gaussian functions. For the phonon modes, functions which were approximately 99.9% Gaussian and 0.1% Lorentzian produced the best fits. The linewidths of phonon modes varied between 2 cm^{-1} (E_g^1) and 20 cm^{-1} (A_{1g}^1). The linewidths of the electronic Raman transitions were between 3 and 6 cm^{-1}. The maximum uncertainties for the intensity measurements are about 5% for $PrVO_4$ and 20% for $NdVO_4$.

III. THEORETICAL ANALYSIS

A. Phonon Raman scattering

The PDI functions corresponding to a phonon mode whose symmetry belongs to any of the 32 point groups can be found in Table I of Ref. 20. We denote by e_1 and e_2 the incident and scattered unit polarization vectors, respectively. Thus the notation α_{21} (see below) refers to the scattered and incident radiation, respectively, reading from left to right. Taking into account the 45° rotation of the RE center about the Z axis and the scattering geometry, in which scattered light is detected at 90° with respect to the incident beam, the polarization-dependent intensities are functions of polarization angles

$$\theta_1,\ \theta_2,\ \varphi_1=-45°,\ \text{and}\ \ \varphi_2=45°, \tag{1}$$

where θ_i and φ_i are the respective polar and azimuth angles of the unit polarization vector e_i with respect to the z axis in the molecular coordinate system.

Noting that in nonresonant scattering, the α_q^1 terms vanish for all phonon modes, the expression for the intensities in D_{4h} symmetry become

A_{1g} mode:

$$|\alpha_{21}(A_{1g})|^2=\cos^2\theta_1\cos^2\theta_2\left(\frac{-\alpha_0^0+\sqrt{2}\alpha_0^2}{\sqrt{3}}\right)^2, \tag{2}$$

$$B_{1g}\ \text{mode:}\quad |\alpha_{21}(B_{1g})|^2=\sin^2\theta_1\sin^2\theta_2\left(\frac{\alpha_2^2+\alpha_{-2}^2}{2}\right)^2,$$

$$B_{2g}\ \text{mode:}\quad |\alpha_{21}(B_{2g})|^2=0,$$

$$E_g\ \text{mode:}\quad |\alpha_{21}(E_{1g})|^2=\left(\frac{\alpha_1^2}{2}\right)^2[\sin^2(\theta_1-\theta_2)+\sin^2(\theta_2+\theta_1)].$$

The polarization dependence of the phonon intensity corresponding to an E_g phonon mode at fixed values of θ_1 has the following simplified forms:

$$|\alpha_{21}(\theta_2,0)|^2=[(\alpha_1^2)^2/2]\sin^2\theta_2, \tag{3}$$

$$|\alpha_{21}(\theta_2,\pm 22.5°)|^2=[(\alpha_1^2)^2/2](0.85\sin^2\theta_2+0.15\cos^2\theta_2),$$

$$|\alpha_{21}(\theta_2,\pm 45°)|^2=[(\alpha_1^2)^2/2],$$

$$|\alpha_{21}(\theta_2,\pm 67.5°)|^2=[(\alpha_1^2)^2/2](0.85\cos^2\theta_2+0.15\sin^2\theta_2),$$

$$|\alpha_{21}(\theta_2,\pm 90°)|^2=[(\alpha_1^2)^2/2]\cos^2\theta_2.$$

A particularly interesting case for the E_g mode occurs when $\theta_1=45°$ as the scattering intensity is a constant, independent of θ_2, and vice versa. This can be conveniently used as a guide to check the alignment of the crystal sample at both room and low temperatures.

B. Electronic Raman scattering

The general formula for the polarization dependence of the Raman scattering tensor α_{21} (where α_{21} is now defined for ERS and is different from the α_{21} described in Sec. III A for phonon scattering) is given by[20]

$$\begin{aligned}\alpha_{21}=&\left(-\frac{1}{\sqrt{3}}\right)[n_2n_1+m_2m_1+l_2l_1]\alpha_0^{(0)}+\left(-\frac{1}{\sqrt{6}}\right)[-2n_2n_1+m_2m_1+l_2l_1]\alpha_0^{(2)}+\frac{1}{2}[(n_2m_1+m_2n_1)i-(n_2l_1+l_2n_1)]\alpha_1^{(2)}\\&+\frac{1}{2}[(n_2m_1+m_2n_1)i+(n_2l_1+l_2n_1)]\alpha_{-1}^{(2)}+\frac{1}{2}[(l_2l_1-m_2m_1)-(l_2m_1+m_2l_1)i]\alpha_2^{(2)}+\frac{1}{2}[(l_2l_1-m_2m_1)\\&+(l_2m_1+m_2l_1)i]\alpha_{-2}^{(2)}+\frac{i}{2}[m_2l_1-l_2m_1]\alpha_0^{(1)}+\frac{1}{2}[(m_2n_1-n_2m_1)i+(n_2l_1-l_2n_1)]\alpha_1^{(1)}\\&+\frac{1}{2}[(-m_2n_1+n_2m_1)i+(n_2l_1-l_2n_1)]\alpha_{-1}^{(1)}.\end{aligned} \tag{4}$$

In Eq. (4), the $\alpha_q^{(t)}$ terms ($t=0,1,2$ and $q=-2,-1,\ldots,2$) are the irreducible second-rank tensors, and

$$(l_i,m_i,n_i)=(\sin\theta_i\cos\varphi_i,\sin\theta_i\sin\varphi_i,\cos\theta_i). \tag{5}$$

The initial and final crystal-field levels can be written in terms of Russell-Saunders coupled wave functions:

$$|i\rangle=\sum_{\alpha SLJJ_z}a(i;nf^N\mu SLJJ_z)|nf^N\mu SLJJ_z\rangle,\quad |f\rangle=\sum_{\alpha' S'L'J'J_z'}a'(f;nf^N\mu' S'L'J'J_z')|nf^N\mu' S'L'J'J_z'\rangle, \tag{6}$$

The second-order expression for the ERS amplitude corresponding to the transition between states $|i\rangle$ and $|f\rangle$ is given by[3,4]

$$\langle i|\alpha_q^{(t)}|f\rangle=F_t^{\mathrm{ERS}}\sum_{\alpha SLJJ_z}\sum_{\alpha' S'L'J'J_z'}a(i;nf^N\mu SLJJ_z)a'(f;nf^N\mu' S'L'J'J_z')\langle nf^N\mu SLJJ_z|\mathbf{U}_q^{(t)}|nf^N\mu' S'L'J'J_z'\rangle, \tag{7}$$

where

$$\begin{aligned}\langle nf^N\mu SLJJ_z|\mathbf{U}_q^{(t)}|nf^N\mu' S'L'J'J_z'\rangle=&(-1)^{2J'+S+L'+t-J_z}[(2J'+1)(2J+1)]^{1/2}\begin{pmatrix}J & t & J'\\ -J_z & q & J_z'\end{pmatrix}\begin{Bmatrix}L & J & S\\ J' & L' & t\end{Bmatrix}\\&\times\langle SL||\mathbf{U}^{(t)}||SL'\rangle\delta(S,S'),\end{aligned} \tag{8}$$

TABLE I. Crystal-field energy levels and wave functions for the ground multiplet of Pr^{3+} in $PrVO_4$.

Energy (cm^{-1})[a]	Energy (cm^{-1})[b]	Symmetry	Wave function $\Sigma_{J,J_z} a(J,J_z)^{2S+1}L_J(J_z)$[a]
0	0	Γ_3	$0.71\,^3H_4(2)+0.71\,^3H_4(-2)$
35		Γ_1	$0.53\,^3H_4(4)+0.53\,^3H_4(-4)+0.67\,^3H_4(0)$
85	84	Γ_5	$0.92\,^3H_4(\pm1)+0.37\,^3H_4(\mp3)$
171		Γ_2	$0.71\,^3H_4(4)-0.71\,^3H_4(-4)$
195		Γ_4	$0.71\,^3H_4(2)-0.71\,^3H_4(-2)$
343		Γ_1	$0.47\,^3H_4(4)+0.47\,^3H_4(-4)-0.75\,^3H_4(0)$
409	342	Γ_5	$-0.92\,^3H_4(\mp3)+0.37\,^3H_4(\pm1)$

[a]From Ref. 24.

[b]Observed energy levels for $PrVO_4$ from the ERS spectra.

and

$$F_t^{\mathrm{ERS}}=(-1)^t\sum_{nf^{N-1}n'l'}7(2l'+1)\begin{pmatrix}3&1&l'\\0&0&0\end{pmatrix}^2\times\langle nf|r|n'l'\rangle^2(2t+1)^{1/2}\begin{Bmatrix}1&3&l'\\3&1&t\end{Bmatrix}\times\left[\frac{1}{E_{l'}-\hbar\omega_i}+\frac{(-1)^t}{E_{l'}+\hbar\omega_s}\right]. \tag{9}$$

In Eq. (9) $n'l'$ is the orbital quantum number of the excited state level, $E_{l'}$ is the difference in energy between configurations $n'l'$ and nl, and $\hbar\omega_i$ and $\hbar\omega_s$ are the respective energies of the incident and scattered photons. Since the initial state is from an f^N configuration, only opposite parity d or g configurations can contribute to the ERS scattering tensor. It is instructive to examine the explicit expressions of F_1 and F_2. Making the approximations $\omega_i\approx\omega_s=\omega$ and $\omega_i\ll E_{l'}$ we have

$$F_1^{\mathrm{ERS}}=-7(3)^{1/2}\sum_{4f^{N-1}n'l'}(2l'+1)\langle 4f|r|n'l'\rangle^2\times\begin{pmatrix}3&1&l'\\0&0&0\end{pmatrix}^2\begin{Bmatrix}1&3&l'\\3&1&1\end{Bmatrix}\frac{2\hbar\omega}{E_{l'}^2},$$

and

$$F_2^{\mathrm{ERS}}=7(5)^{1/2}\sum_{4f^{N-1}n'l'}(2l'+1)\langle 4f|r|n'l'\rangle^2\times\begin{pmatrix}3&1&l'\\0&0&0\end{pmatrix}^2\begin{Bmatrix}1&3&l'\\3&1&2\end{Bmatrix}\frac{2}{E_{l'}}. \tag{10}$$

We now compare separately the contributions of the d and g orbital configurations.

For the d orbitals:

$$F_{1d}^{\mathrm{ERS}}=\frac{\sqrt{6}}{\sqrt{7}}\sum_{4f^{N-1}5d}\langle 4f|r|5d\rangle^2\frac{2\hbar\omega}{E_d^2},$$

and

$$F_{2d}^{\mathrm{ERS}}=\frac{3\sqrt{2}}{\sqrt{35}}\sum_{4f^{N-1}5d}\langle 4f|r|5d\rangle^2\frac{2}{E_d}. \tag{11}$$

For the g orbitals:

$$F_{1g}^{\mathrm{ERS}}=-\frac{2\sqrt{3}}{\sqrt{14}}\sum_{4f^{N-1}5g}\langle 4f|r|5g\rangle^2\frac{2\hbar\omega}{E_g^2},$$

and

$$F_{2g}^{\mathrm{ERS}}=\frac{2\sqrt{5}}{3\sqrt{14}}\sum_{4f^{N-1}5g}\langle 4f|r|5g\rangle^2\frac{2}{E_g}. \tag{12}$$

TABLE II. Crystal-field energy levels and wave functions for the ground multiplet of Nd^{3+} in $NdVO_4$.

Energy (cm^{-1})[a]	Energy (cm^{-1})[b]	Symmetry	Wave function $\Sigma_{J,J_z} a(J,J_z)^{2S+1}L_J(J_z)$[c]
0	0	Γ_7	$0.77\,^4I_{9/2}(1/2)-0.61\,^4I_{9/2}(-7/2)$
108	101	Γ_7	$-0.77\,^4I_{9/2}(-7/2)-0.60\,^4I_{9/2}(1/2)$
175	169	Γ_6	$0.83\,^4I_{9/2}(3/2)-0.53\,^4I_{9/2}(-5/2)$
219	178	Γ_7	$-0.98\,^4I_{9/2}(9/2)+0.17\,^2H2_{9/2}(9/2)$
437		Γ_6	$-0.83\,^4I_{9/2}(-5/2)-0.52\,^4I_{9/2}(3/2)$

[a]From Ref. 25.

[b]Observed energy levels for $NdVO_4$ from the ERS spectra.

[c]From Ref. 25. Only half of the Kramers' doublet is listed.

TABLE III. Matrix elements of the irreducible ERS tensors calculated in the second order for the $^3H_4$ ground multiplet of Pr^{3+} in $PrVO_4$.

Transitions	$\alpha_q^t=\langle i\|\alpha_q^{(t)}\|f\rangle$
0-35	$\alpha_2^2=\alpha_{-2}^2=0.118F_2$
0-84	$\alpha_1^2=0.031F_2,\ \alpha_1^1=-0.346F_1$
0-171	$\alpha_2^2=\alpha_{-2}^2=0.050F_2$
0-195	$\alpha_0^1=0.261F_1$
0-343	$\alpha_2^2=\alpha_{-2}^2=-0.062F_2$
0-409	$\alpha_1^2=0.145F_2,\ \alpha_1^1=0.122F_1$

Assuming the degeneracy of the g and d orbital configuration energy levels, the ratio F_1/F_2 is given by the relation

$$\tau=\frac{F_1}{F_2}=\frac{F_{1d}+F_{1g}}{F_{2d}+F_{2g}}=\frac{\sqrt{3}}{\sqrt{5}}\,\hbar\omega\,\frac{(1/E_d^2-R/E_g^2)}{(3/5E_d+R/3E_g)},\quad(13)$$

where

$$R=\frac{|\langle 4f|r|5g\rangle|^2}{|\langle 4f|r|5d\rangle|^2}.\quad(14)$$

The expression for the ERS amplitude can be expanded in the third order to include the spin-orbit interaction. The irreducible scattering tensor corresponding to the third-order spin-orbit interaction has the form[11]

$$(\alpha_q^{(t)})^{3\mathrm{rd}}=H(t)(\mathbf{a}^\dagger\mathbf{a})_q^{(0t)t}(\mathbf{a}^\dagger\mathbf{a})^{(11)0}+\sum_\lambda G(t,\lambda)(\mathbf{a}^\dagger\mathbf{a})_q^{(1\lambda)t},\quad(15)$$

where $\mathbf{a}^\dagger$, $\mathbf{a}$ represent creation and annihilation tensors, and $t=0$, 1, or 2. $H(t)$ and $G(t,\lambda)$ have the following expressions for $l=3$ and $l'=2$:

$$H(0)=\frac{6\zeta_f}{E_{df}^2}(f|r|d)^2,\quad H(1)=\frac{2\sqrt{6}\zeta_f}{E_{df}^2}(f|r|d)^2,\quad(16)$$

$$H(2)=\frac{6\sqrt{6}\zeta_f}{5E_{df}^2}(f|r|d)^2,$$

$$G(0,1)=\frac{(6\zeta_f-4\zeta_d)}{\sqrt{14}E_{df}^2}(f|r|d)^2,$$

$$G(1,1)=\frac{-\zeta_f}{\sqrt{14}E_{df}^2}(f|r|d)^2,$$

TABLE IV. Matrix elements of the irreducible ERS tensors calculated in the second order for the $^4I_{9/2}$ ground multiplet of Nd^{3+} in $NdVO_4$.

Transitions (cm^{-1})	$\alpha_q^t=\langle i\|\alpha_q^{(t)}\|f\rangle$
0-108	$\alpha_0^2=0.0395F_2,\ \alpha_0^1=-0.259F_1$ $\alpha_1^2=0.000F_2$ $\alpha_1^1=0.229F_1$
0-175	$\alpha_1^2=-0.004F_2,\ \alpha_1^1=0.432F_1$ $\alpha_2^2=-0.053F_2,\ \alpha_{-2}^2=0.045F_2$
0-219	$\alpha_1^2=0.041F_2,\ \alpha_1^1=0.175F_1$
0-437	$\alpha_1^2=-0.046F_2,\ \alpha_1^1=-0.003F_1$ $\alpha_2^2=-0.015F_2,\ \alpha_{-2}^2=-0.029F_2$

$$G(1,2)=\frac{(5\zeta_f-4\zeta_d)\sqrt{3}}{\sqrt{70}E_{df}^2}(f|r|d)^2,$$

$$G(2,1)=\frac{(-18\zeta_f+8\zeta_d)}{\sqrt{1400}E_{df}^2}(f|r|d)^2,$$

$$G(2,2)=\frac{-3\sqrt{42}\zeta_f}{70E_{df}^2}(f|r|d)^2,$$

$$G(2,3)=\frac{3\sqrt{42}(\zeta_f-\zeta_d)}{35E_{df}^2}(f|r|d)^2.$$

The first term on the right-hand side of Eq. (15) is a scalar product of coupled tensors. Since this term can connect nonidentical initial and final states, the matrix element $\alpha_0^{(0)}$ no longer vanishes. For $t=0$, $\alpha_0^{(0)}$ can be decomposed into two terms:

$$\alpha_0^{(0)}=S_{00}+S_{01},\quad(17)$$

where

$$S_{00}=H(0)(\mathbf{a}^\dagger\mathbf{a})_0^{(00)0}(\mathbf{a}^\dagger\mathbf{a})^{(11)0}$$

and (18)

$$S_{01}=G(0,1)(\mathbf{a}^\dagger\mathbf{a})_0^{(11)0}.$$

Since the eigenvalue of $(\mathbf{a}^\dagger\mathbf{a})_0^{(00)0}$ is $-N(14)^{-1/2}$ when coupling states $(l^NSLJJ_z|$ and $|l^NS'L'J'J_z')$, the first term of $\alpha_0^{(0)}$ becomes $N(14)^{-1/2}H(0)\mathbf{W}_0^{(11)0}$, where $\mathbf{W}_q^{(1\lambda)t}$ represents the standard sum of single-particle double-tensor operators.

The total third-order spin-orbit contribution for the case $t=0$ is given by

TABLE V. Energies (cm^{-1}) and symmetry irreducible representations of the Raman-active phonons in $PrVO_4$ at 297 and 4.2 K. (-) indicates not observed.

Temp.	E_g^1	B_{1g}^1	E_g^2	E_g^3	B_{1g}^2	B_{2g}^1	A_{1g}^1	E_g^4	B_{1g}^3	B_{1g}^4	E_g^5	A_{1g}^2
297 K	113	122	150	233	261		381	-	470	792	805	869
4.2 K	116	115	152	231	260		377	-	469	797	807	872

$$(l^N SLJM|(\alpha_0^0)^{3\mathrm{rd}}|l^N S'L'J'M') = (l^N SLJM|S_{00}+S_{01}|l^N S'L'J'M')$$

$$= \left[\frac{N}{\sqrt{14}}H(0) - G(0,1)\right](-1)^{J-M}\begin{pmatrix} J & 0 & J' \\ -M & 0 & M' \end{pmatrix}(l^N SLJ\|\mathbf{W}^{(11)0}\|l^N S'L'J'). \tag{19}$$

For $t=1$ and $\lambda=0,1,2$, $\alpha_q^{(1)}$ contains three terms:

$$\alpha_q^{(1)} = S_{10}+S_{11}+S_{12}, \tag{20}$$

where

$$S_{10} = H(1)(\mathbf{a}^\dagger\mathbf{a})_q^{(01)1}(\mathbf{a}^\dagger\mathbf{a})^{(11)0} = H(1)\mathbf{W}^{(11)0}\sqrt{\tfrac{3}{2}}\mathbf{U}_q^{(1)},$$

$$S_{11} = G(1,1)(\mathbf{a}^\dagger\mathbf{a})_q^{(11)1}, \quad \text{and} \quad S_{12} = G(1,2)(\mathbf{a}^\dagger\mathbf{a})_q^{(12)1}. \tag{21}$$

The total third-order spin-orbit contribution for the case $t=1$ is given by

$$\begin{aligned}(l^N\alpha SLJM|S_{10}+S_{11}+S_{12}|l^N\alpha' S'L'J'M') = (-1)^{J-M}\begin{pmatrix} J & 1 & J' \\ -M & q & M' \end{pmatrix}&\left[\sqrt{\tfrac{3}{2}}H(1)[J']^{-1/2}(l^N\alpha SLJ\|\mathbf{U}^{(1)}\|l^N\alpha SLJ)\right.\\ &\times(l^N\alpha SLJ\|\mathbf{W}^{(11)0}\|l^N\alpha' S'L'J') - G(1,1)(l^N\alpha SLJ\|\mathbf{W}^{(11)1}\|l^N\alpha' S'L'J')\\ &\left.- G(1,2)(l^N\alpha SLJ\|\mathbf{W}^{(12)1}\|l^N\alpha' S'L'J')\right]\end{aligned} \tag{22}$$

For $t=2$ and $\lambda=0,1,2,3$, $\alpha_q^{(1)}$ contains four terms:

$$\alpha_q^{(2)} = S_{20}+S_{21}+S_{22}+S_{23} \tag{23}$$

where

$$S_{20} = H(2)(\mathbf{a}^\dagger\mathbf{a})_q^{(02)2}(\mathbf{a}^\dagger\mathbf{a})^{(11)0} = H(2)\mathbf{W}^{(11)0}\sqrt{\tfrac{5}{2}}\mathbf{U}_q^{(2)},$$

$$S_{21} = G(2,1)(\mathbf{a}^\dagger\mathbf{a})_q^{(11)2}, \quad S_{22} = G(2,2)(\mathbf{a}^\dagger\mathbf{a})_q^{(12)2}, \quad \text{and} \quad S_{23} = G(2,3)(\mathbf{a}^\dagger\mathbf{a})_q^{(13)2}. \tag{24}$$

The total third-order spin-orbit contribution for the case $t=2$ is given by

$$\begin{aligned}&(l^N\alpha SLJM|S_{20}+S_{21}+S_{22}+S_{23}|l^N\alpha' S'L'J'M')\\ &= (-1)^{J-M}\begin{pmatrix} J & 2 & J' \\ -M & q & M' \end{pmatrix}\left[\sqrt{\tfrac{5}{2}}\,H(2)[J']^{-1/2}\sum_{\alpha''L''}(l^N\alpha SLJ\|\mathbf{U}^{(2)}\|l^N\alpha'' SL''J')(l^N\alpha'' SL''J'\|\mathbf{W}^{(11)0}\|l^N\alpha' S'L'J')\right.\\ &- G(2,1)(l^N\alpha SLJ\|\mathbf{W}^{(11)2}\|l^N\alpha' S'L'J') - G(2,2)(l^N\alpha SLJ\|\mathbf{W}^{(12)2}\|l^N\alpha' S'L'J')\\ &\left.- G(2,3)(l^N\alpha SLJ\|\mathbf{W}^{(13)2}\|l^N\alpha' S'L'J')\right].\end{aligned} \tag{25}$$

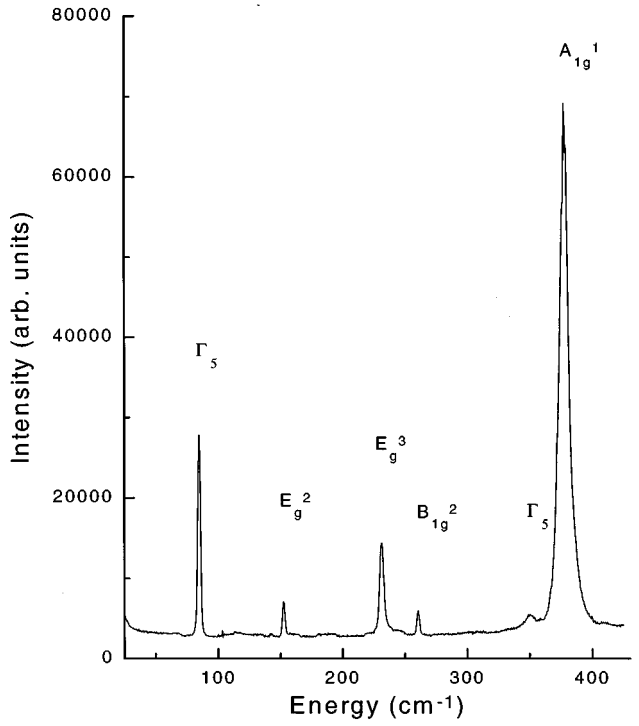

FIG. 1. Low-temperature, unpolarized ERS spectrum of $PrVO_4$ with 514 nm excitation.

Since the ERS amplitude corresponding to the third-order spin-orbit contribution can be expressed in terms of the second-rank irreducible tensors [Eq. (15)], its polarization-dependent form is the same as that of the second order. We can therefore just add $\langle i|\alpha_q^{(t)}|f\rangle$ calculated in the third order to the second-order values and square the value of $\langle i|\alpha_{21}|f\rangle$ [Eq. (4)] to obtain the ERS intensity calculated up to the third order involving spin-orbit coupling.

The wave functions for Pr^{3+} ions in $PrVO_4$ are shown in Table I. These wave functions were obtained from a crystal-field calculation using the crystal-field parameters given by Andronenko *et al.*[24] The wave functions for Nd^{3+} ions in $NdVO_4$ listed in Table II were given by Tanner and Edelstein.[25] These wave functions were obtained from a crystal-field fit using the observed energy levels of Nd^{3+} ions diluted in YVO_4:Nd^{3+}. The calculated nonzero values for the matrix elements of $\alpha_q^{(t)}$ for Pr^{3+} ions in $PrVO_4$ and Nd^{3+} ions in $NdVO_4$ are shown in Tables III and IV, respectively.

A particular electronic Raman transition of interest in $PrVO_4$ is the first Γ_3-Γ_5 transition at 85 cm^{-1}. The polarization-dependent ERS intensity corresponding to this transition is proportional to

$$\begin{aligned}|\alpha_{21}(\Gamma_3\rightarrow\Gamma_5)|^2 &= \tfrac{1}{4}\{[\alpha_1^2\sin(\theta_2+\theta_1)+\alpha_1^1\sin(\theta_2-\theta_1)]^2 \\ &+[\alpha_1^1\sin(\theta_2+\theta_1)+\alpha_1^2\sin(\theta_2-\theta_1)]^2\} \\ &+\tfrac{1}{4}\{[\alpha_{-1}^2\sin(\theta_2+\theta_1)\ -\alpha_{-1}^1\sin(\theta_2-\theta_1)]^2 \\ &+[-\alpha_{-1}^1\sin(\theta_2+\theta_1)+\alpha_{-1}^2\sin(\theta_2-\theta_1)]^2\},\end{aligned} \tag{26}$$

where the left-hand side of Eq. (26) denotes the squared ERS amplitude for the transition, and the α_q^t terms denote the matrix elements of the $\alpha_q^{(t)}$ tensors, $\langle\Gamma_3|\alpha_q^{(t)}|\Gamma_5\rangle$.

Noting the fact that the squared amplitude must be the same for electronic Raman transitions coming from a singlet to each state of the doubly degenerate level,[20] Eq. (26) becomes

$$\begin{aligned}|\alpha_{21}(\Gamma_3\rightarrow\Gamma_5)|^2 &= \tfrac{1}{2}\{[\alpha_1^2\sin(\theta_2+\theta_1)+\alpha_1^1\sin(\theta_2-\theta_1)]^2 \\ &+[\alpha_1^1\sin(\theta_2+\theta_1)+\alpha_1^2\sin(\theta_2-\theta_1)]^2\}.\end{aligned} \tag{27}$$

If we define

$$a=\frac{\alpha_1^2}{\alpha_1^1}=-\frac{\alpha_{-1}^2}{\alpha_{-1}^1}=-0.09\frac{F_2}{F_1}=\frac{-0.09}{\tau}, \tag{28}$$

the squared amplitude of the scattering tensor for the transition becomes

$$\begin{aligned}|\alpha_{21}(\Gamma_3\rightarrow\Gamma_5)|^2 &= \frac{(\alpha_1^1)^2}{2}\{[\sin^2(\theta_2+\theta_1)+\sin^2(\theta_2-\theta_1)] \\ &\times(a^2+1)+4a\ \sin(\theta_2+\theta_1) \\ &\times\sin(\theta_2-\theta_1)\}.\end{aligned} \tag{29}$$

We now keep θ_1 fixed at values incremented by 22.5° and determine the scattered intensity with respect to θ_2. For each value of θ_1,

$$\begin{aligned}|\alpha_{21}(0,\theta_2)|^2 &= [(\alpha_1^1)^2](a+1)^2\sin^2\theta_2, \\ |\alpha_{21}(\pm 22.5°,\theta_2)|^2 &= [(\alpha_1^1)^2][0.85(a+1)^2\sin^2\theta_2 \\ &+0.15(a-1)^2\cos^2\theta_2], \\ |\alpha_{21}(\pm 45°,\theta_2)|^2 &= \frac{[(\alpha_1^1)^2]}{2}(a^2+1-2a\ \cos 2\theta_2), \\ |\alpha_{21}(\pm 67.5°,\theta_2)|^2 &= [(\alpha_1^1)^2][0.85(a-1)^2\cos^2\theta_2 \\ &+0.15(a+1)^2\sin^2\theta_2], \\ |\alpha_{21}(\pm 90°,\theta_2)|^2 &= [(\alpha_1^1)^2](a-1)^2\cos^2\theta_2.\end{aligned} \tag{30}$$

The polarization-dependent ERS intensity for the Γ_7-Γ_7 transition at 101 cm^{-1} in $NdVO_4$ is proportional to

$$\begin{aligned}|\alpha_{21}(\Gamma_7\rightarrow\Gamma_7)|^2 &= (\alpha_0^1)^2\sin^2\theta_1\sin^2\theta_2+\tfrac{2}{3}[2(\alpha_0^2)^2+(\alpha_0^0)^2] \\ &\times\cos^2\theta_1\cos^2\theta_2+\tfrac{1}{4}(\alpha_1^1)^2[\sin^2(\theta_2+\theta_1) \\ &+\sin^2(\theta_2-\theta_1)].\end{aligned} \tag{31}$$

IV. $PrVO_4$ EXPERIMENTAL RESULTS AND DISCUSSION

Table V lists all the phonon modes observed for the $PrVO_4$ crystal at room temperature and at 4.2 K. These phonon modes were assigned based on their PDI behavior described in Eqs. (2). Figure 1 shows the unpolarized spectrum for the phonon and electronic Raman transitions in $PrVO_4$ between 30 and 450 cm^{-1}, which were recorded at 4.2 K

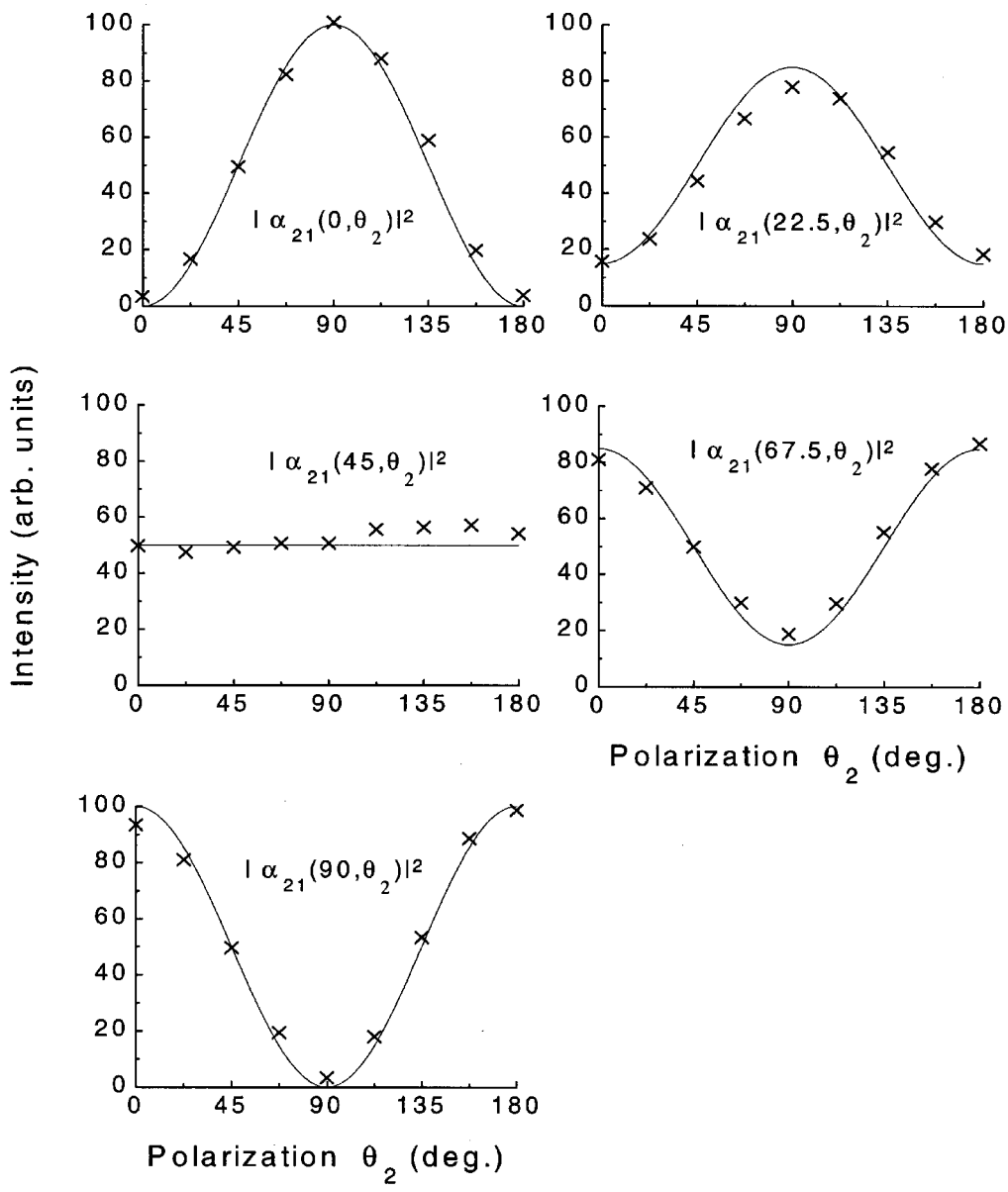

FIG. 2. Low-temperature polarization dependence of the intensity of the E_g^5 phonon of $PrVO_4$ with 514 nm excitation. Solid lines represent the fitted curves using Eqs. (3); crosses represent the experimental data.

using the 514 nm excitation line. The capital Roman symbols represent the phonon modes, and the capital Greek letters represent the electronic Raman transitions. Only two electronic levels at 84 and 344 cm^{-1} were observed, both of which were assigned to the symmetry representation Γ_5, as their intensities were strongest in XZ and ZY scans. ''XZ'' and ''ZY'' correspond to the polarization states ($\theta_1=0$, $\theta_2=90$) and ($\theta_1=90$, $\theta_2=0$), respectively. The assignment for the first doublet transition is in good agreement with reported fluorescence data,[26] in which the first doublet level was assigned at 84 cm^{-1}. Our assignment for the second electronic Raman transition, however, disagrees with the predicted assignment given by Andronenko *et al.*[24] Based on their assignments, a single transition should have appeared at approximately 343 cm^{-1}, and a second doublet transition should have been observed at 409 cm^{-1}. Our theoretical assignments using a crystal-field calculation with the crystal-field parameters given by Ref. 24 showed that the first and second doublet transitions would be located at 70 cm^{-1} and 373 cm^{-1}, respectively. The difference in energy levels between theory and observation should not be overemphasized, as we note that the crystal-field parameters used to calculate the energy levels come from a crystal-field fit which included only two empirical energy levels. No other electronic lines were found in either polarized or unpolarized scans using the 488, 496, and 501 nm excitation lines.

For calibration purposes, PDI spectra have been recorded for the phonon mode at 807 cm^{-1}. It was selected because it exhibits similar polarization behavior to the electronic Raman transition at 84 cm^{-1} and it also has a comparatively large oscillator strength. PDI ERS spectra were obtained for the first doublet transition at 84 cm^{-1}, whose intensity is strong enough for reliable polarization measurements. The phonon lines in Fig. 1 are located away from the electronic

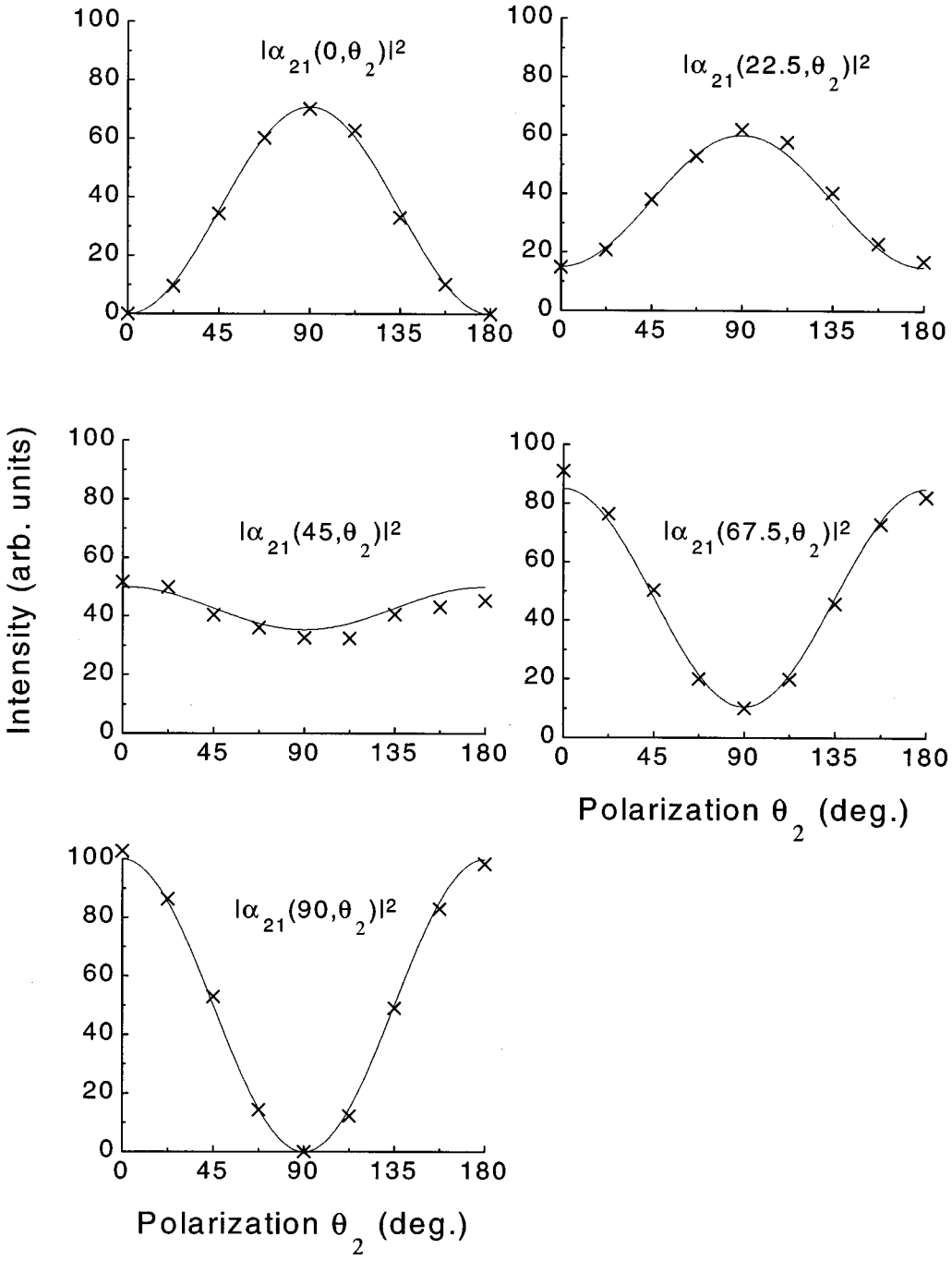

FIG. 3. Low-temperature polarization dependence of the intensity of the electronic Raman transition at 84 cm^{-1} of Pr^{3+} in $PrVO_4$ with 514 nm excitation. Solid lines represent the fitted curves using Eqs. (30); crosses represent the calibrated data.

line at 84 cm^{-1} and do not seem to show an electron-phonon coupling effect.

The ERS intensities were calibrated and fitted using the calibration procedure described in Ref. 19. Figure 2 shows the polarization-dependent intensities of the E_g^5 phonon mode at 807 cm^{-1} and its predicted intensities described by Eqs. (3). Figure 3 displays the calibrated PDI curves for the electronic Raman transition at 84 cm^{-1} and the corresponding fitted curves given in Eqs. (30). The fitted value of $a = \alpha_1^2/\alpha_1^1$ appearing in the PDI functions was obtained from the least-squares fit of the ERS data to the corresponding functions given in Eqs. (30). The observed and predicted data in Figs. 2 and 3 were scaled in such a way that the maximum values of the predicted data are 100. The observed data for the polarization-dependent ERS and phonon spectra agree well with prediction. Good agreement was expected since the polarization-dependent form of the scattering tensor described in expression (27) has been obtained purely from group theoretical considerations. The Judd-Ofelt-Axe approximation was not introduced until the evaluation of the ratio α_1^2/α_1^1 in terms of $\tau = F_1/F_2$, which appears later in Eq. (29).

Two fitted values of α_1^2/α_1^1 for the doublet transition at 84 cm^{-1} were extracted from the least-squares analysis using

TABLE VI. Comparison between calculated and observed relative line strengths of electronic Raman transitions in the $^3H_4$ ground multiplet of Pr^{3+} in $PrVO_4$ for the case $\tau=1.03$. Estimated maximum uncertainties for the intensity measurements are less than 5%. (-) indicates not observed.

Transitions (cm^{-1})		ZZ polarized		XY polarized		XZ polarized		ZY polarized	
Cal.[a]	Exp.	Cal.	Obs.	Cal.	Obs.	Cal.	Obs.	Cal.	Obs.
35	-	0	-	0.18	-	0	-	0	-
85	84	0	-	0	-	0.70	0.71	1.0	1.0
171	-	0	-	0	-	0	-	0	-
195	-	0	-	0.23	-	0	-	0	-
343	-	0	-	0.05	-	0	-	0	-
409	344	0	-	0	-	0.47	0.25	0.002	-

[a]From Ref. 24, see Table I.

a total of 45 data points. These fitted values are the quadratic solutions of Eq. (29) and were found to be -0.0865 and -11.57. The corresponding values of τ are 1.04 and 0.0078, respectively. Including only the d configuration and assuming that $E_d(Pr^{3+})=50\,000\ cm^{-1}$ and $\hbar\omega=20\,000\ cm^{-1}$, the calculated values for $a=\alpha_1^2/\alpha_1^1$ and τ are -0.175 and 0.52, respectively. The fact that one of the fitted values of τ (and a) only differs by a factor of 2 with the prediction from the second-order perturbation theory of Axe demonstrates the dominance of the d configuration in accounting for the two-photon intensities in $PrVO_4$.

Table VI compares the observed and predicted relative line strengths for the case $\tau=1.03$. It is clear that a value $\tau\cong 1$ accounts for the relative line strengths observed and explains the absence of most of the other electronic Raman transitions originating in the electronic ground state.

From the analysis above we conclude that the value of τ is most likely near unity. The other value of τ coming from the fit does not account for the observed intensities and is thus considered nonphysical. This result is not in agreement with the earlier results of Becker *et al.*,[6,7] for $TmPO_4$, who reported that $\tau=F_1/F_2\sim 0$. From the deduced small value for τ, Becker *et al.* suggested that the excited g configuration may make an important contribution to two-photon intensities.[27] As can be seen from Eq. (13), if only the d-orbital configuration is taken into account, and using the values of R and E_d given by the Hartree-Fock calculation for the free ion, the ratio F_1/F_2 is approximately 0.25 for the Tm^{3+} ion, which is an order of magnitude larger than their empirical values. Becker *et al.* asserted that a value of magnitude -0.03 for this ratio can only be obtained when the second term in the numerator of Eq. (13) is comparable to the first term, which suggests that the g-orbital configuration might play an important role in two-photon processes. In our analysis for $PrVO_4$ the contribution from the d-orbital configuration alone is sufficient to account for most transition intensities in the ground multiplet and for the PDI behavior of the electronic Raman transition at 84 cm^{-1} in $PrVO_4$.

It remains to consider other possible contributions to the ERS intensities. These contributions include third- and fourth-order interactions such as spin-orbit, crystal-field, ligand polarization, and electron-correlation interactions. Using the spin-orbit parameter for the Pr^{3+} ion in YPO_4,[28] we have computed the third-order spin-orbit contribution for the electronic Raman transitions in the ground multiplet. These contributions turn out to be at most an order of magnitude smaller than the second-order contributions and therefore would not significantly affect the results obtained above. For the Pr^{3+} ion both the small third-order term $\langle {}^3H_4\|U^{(2)}W^{(11)0}\|{}^3H_4\rangle$ compared with the second-order term $\langle {}^3H_4\|U^{(2)}\|{}^3H_4\rangle$ and the relatively small spin-orbit constant are the reasons for the small magnitude of the third-order term relative to the second-order contribution. Table VII compares the third-order spin-orbit contribution to the second-order contribution for the doublets at 84 and 344 cm^{-1}.

Although we were not able to compute the third- and fourth-order contributions of other interactions, we do not expect significant changes in our analysis given thus far. First, the PDI behavior will look exactly the same when higher-order terms are added into the second-order term. This is because the PDI function for the transition at 84 cm^{-1} depends on only one variable, namely $a=\alpha_1^2/\alpha_1^1$, which is related to $\tau=F_1/F_2$. Adding higher-order terms only changes the computed values of a and τ, but the general PDI expression for this transition will be the same. Secondly, as noted above, unless the second-order term is negligibly small, which is not the case for the Pr^{3+} ion, in general the contributions to the ERS intensities would decrease rapidly beyond the second order, therefore the values of a and τ should not be very different from the second-order values when higher-order terms have been added. This is not the case for the Gd^{3+} ion, whose leading contribution to two-

TABLE VII. Relative magnitude of third-order spin-orbit to second-order contributions for electronic Raman transitions in $PrVO_4$.

Transitions (cm^{-1})	$(\alpha_1^2)^{3rd}/(\alpha_1^2)^{2nd}$	$(\alpha_1^1)^{3rd}/(\alpha_1^1)^{2nd}$	$(\alpha_1^2/\alpha_1^1)^{2nd}$	$(\alpha_1^2/\alpha_1^1)^{tot}$	$(\alpha_1^2/\alpha_1^1)^{fitted}$	τ^{2nd}	τ^{fitted}
84	-0.036	-0.072	-0.175	-0.181	-0.089	0.52	1.04
344	-0.036	-0.072	2.32	2.40	1.00	0.52	1.20

TABLE VIII. Energies (cm^{-1}) and symmetry irreducible representations of the Raman-active phonons in $NdVO_4$ at 297 and 4.2 K. (-) indicates not observed.

Temp.	E_g^1	B_{1g}^1	E_g^2	E_g^3	B_{1g}^2	B_{2g}^1	A_{1g}^1	E_g^4	B_{1g}^3	B_{1g}^4	E_g^5	A_{1g}^2
297 K	113	123	148	237	260	375	381	-	472	795	808	871
4.2 K	111	121	151	242	259	378	380	-	473	797	810	873

photon intensities is zero in the second order. In this case, adding the third- or higher-order contributions drastically changes the result as demonstrated by Downer *et al.*[9,10]

V. $NdVO_4$ EXPERIMENTAL RESULTS AND DISCUSSION

The observed phonon modes in $NdVO_4$ are listed in Table VIII. All the phonon modes except the B_{2g}^1 mode were clearly identified from their polarization behavior. According to Eqs. (2), a phonon mode of B_{2g} character cannot be observed for the scattering geometry used in these experiments. At room temperature, however, a weak line was observed at 375 cm^{-1} in the XY scan, while no feature appears between 375 and 385 cm^{-1} in the XZ and ZY scans. At 4.2 K the observed linewidth of the A_{1g}^1 mode at 380 cm^{-1} is unusually large in an unpolarized scan, which is attributed to two superimposed phonon modes separated by approximately 2 cm^{-1}. From these observations we assign the Raman line at 378 cm^{-1} to B_{2g}^1 whose observed intensity may arise from imperfect crystal orientation. The E_g^4 mode has never been observed. Polarized Raman spectra of $NdVO_4$ were recorded at room temperature and at 4.2 K using the 488 nm excitation line. Figure 4 shows the unpolarized spectrum for the Raman transitions between 90 and 490 cm^{-1} in $NdVO_4$, taken at 4.2 K using laser excitation at 476 nm. The line appearing at 358 cm^{-1} in Fig. 4 is absent in unpolarized spectra using other laser excitation lines and therefore is assigned as an extraneous feature.

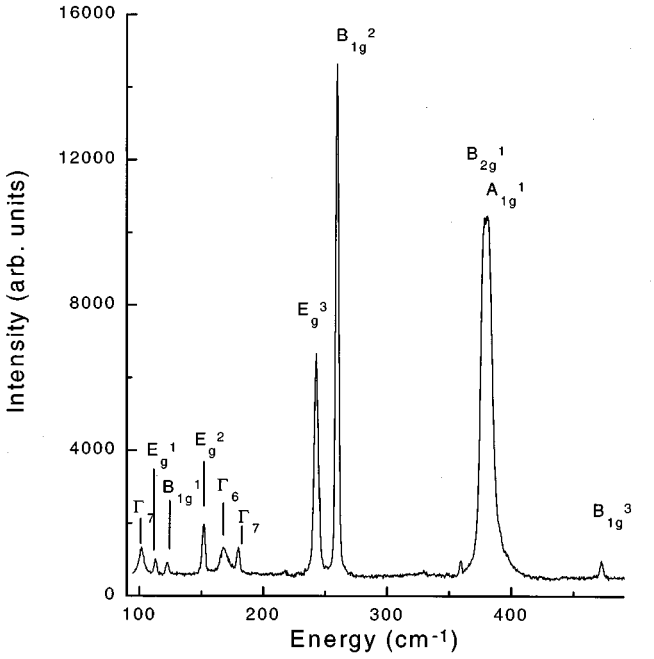

FIG. 4. Low temperature unpolarized ERS spectrum of $NdVO_4$ with 476 nm excitation.

Three electronic Raman transitions were observed and labeled by their symmetry irreducible representations in Fig. 4. These lines were assigned according to their PDI behavior determined by Eq. (4) and Table IV. For example, the intensity of the first transition at 101 cm^{-1} is strongest when $\theta_1 = \theta_2 = 90°$ and weakest, but not zero, when $\theta_1 = \theta_2 = 0°$. This is consistent with the first $\Gamma_7 \rightarrow \Gamma_7$ transition predicted to be at 107 cm^{-1}. Similarly, we assigned the second and third electronic lines to the $\Gamma_7 \rightarrow \Gamma_6$ and $\Gamma_7 \rightarrow \Gamma_7$ transitions, predicted to be at 175 cm^{-1} and 219 cm^{-1}, respectively.

PDI spectra have been recorded for the A_{1g}^2 mode at 875 cm^{-1} and for the observed electronic Raman transition at 101 cm^{-1}. In this case phonon intensities were not used to calibrate the ERS intensities because the polarization curves of all the phonon modes were considerably different from those of the electronic Raman transition. Figures 5 and 6 display the respective experimental PDI behavior of the A_{1g}^2 mode and the electronic Raman transition at 101 cm^{-1}. The predicted curves from Eqs. (2) and (31) are also shown.

A least-squares fit of the intensity data of the electronic Raman transition at 101 cm^{-1} was performed. Since $\alpha_1^2 = 0$ for this transition, we could only obtain the fitted values for α_1^1/α_0^1, α_1^1/α_0^2, and α_0^1/α_0^2. Using the second-order expressions of α_q^t in terms of F_t (Table IV), two values of $\tau = F_1/F_2$ could be extracted from the fitted values of α_1^1/α_0^2 and α_0^1/α_0^2. These values of τ were in turn compared with the predicted values, which were obtained from the second-order theory of Axe including only the d configuration. The fitted value of $|\tau|$ is found to be approximately 0.48, compared to a predicted value of $\tau = 0.43$, assuming $E_d = 60\,000$ cm^{-1} and $\hbar\omega = 20\,000$ cm^{-1} [Eq. (13)]. The fitted and calculated values for α_1^1/α_0^1 differ by less than 10%. All these values are compared in Table IX for the transition at 101 cm^{-1}.

The other two observed electronic Raman transitions had weaker intensities and were spectrally close to each other and to the strong E_g^2 phonon mode at 151 cm^{-1}, which made it very difficult to perform accurate intensity measurements. As a result their recorded intensities were not used in the PDI analysis of $NdVO_4$.

We can now use the fitted value of τ from the transition at 101 cm^{-1} to predict the intensities of the other transitions in the $^4I_{9/2}$ ground multiplet. Table X compares the predicted and observed relative intensities for different transitions for the case $\tau = 0.48$. The agreement between theory and experiment is good for all transitions in the $^4I_{9/2}$ ground multiplet of $NdVO_4$. As was the case of $PrVO_4$, this agreement shows the second-order theory of Axe is sufficient. Since more nonvanishing α_q^t parameters are associated with a transition between two Kramers' states than with a transition between two non-Kramers' states, ERS measurements on Kramers'

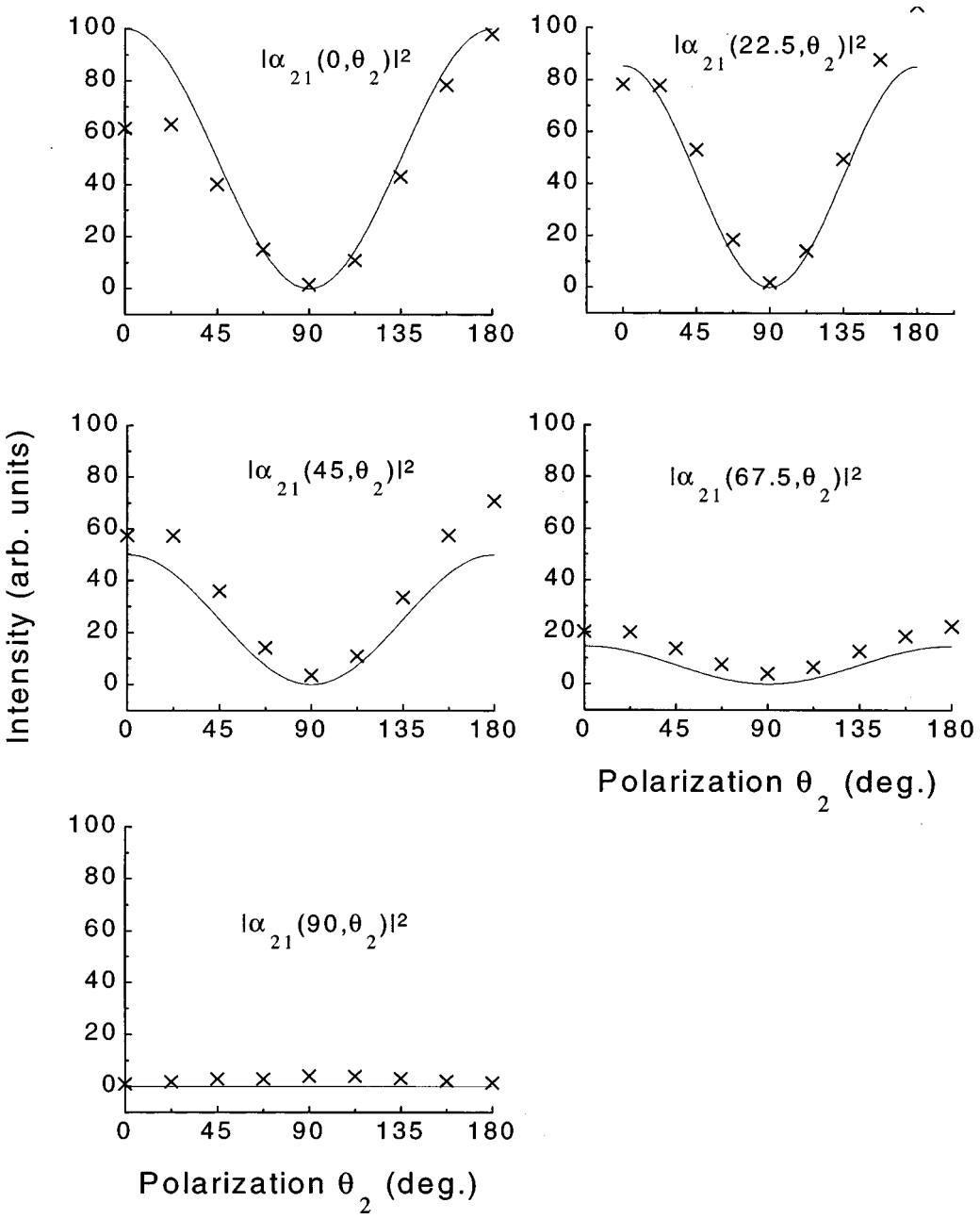

FIG. 5. Low-temperature polarization dependence of the intensity of the A_{1g}^2 phonon mode of $NdVO_4$ with 488 nm excitation. Solid lines represent the fitted curves using Eqs. (2); crosses represent the experimental data.

ions (such as Nd^{3+}) provide a stronger test of Axe's theory.

Table XI shows the relative magnitude of the third-order spin-orbit contribution relative to the second-order contribution. As in the case of $PrVO_4$, the third-order spin-orbit contribution was found to be relatively small compared to the second-order contribution, and the calculated values for α_q^t only changed slightly when the third-order term was included. For Kramers' ions, it might be expected that all

TABLE IX. Comparison of the fitted and calculated values for the relative magnitudes of α_q^t's for the electronic Raman transition in $NdVO_4$ at 101 cm^{-1}. Estimated maximum uncertainties for the intensity measurements are about 20%.

Transition ($101\ cm^{-1}$)	α_0^0	α_1^2	$(\alpha_0^1/\alpha_1^1)^2$	$(\alpha_0^1/\alpha_0^2)^2$, τ	$(\alpha_1^1/\alpha_0^2)^2$, τ
Fitted values	0	0	0.73	10.2, $\pm$0.49	7.4, $\pm$0.47
Calculated values	0	0	0.78	8.0, 0.43	6.2, 0.43

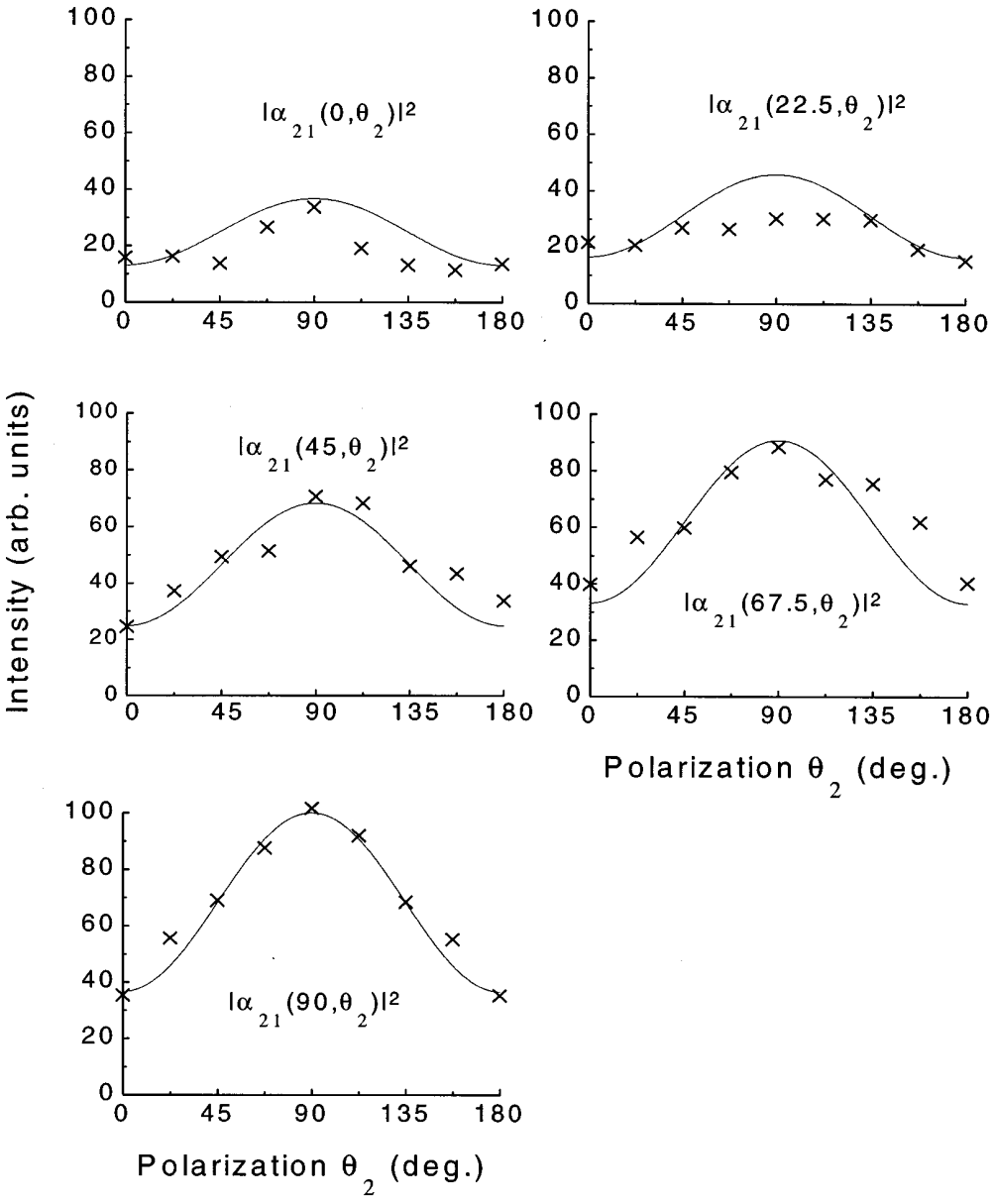

FIG. 6. Low-temperature polarization dependence of the intensity of the electronic Raman transition at 101 cm^{-1} for Nd^{3+} in $NdVO_4$ with 488 nm excitation. Solid lines represent the fitted curves using Eq. (31); crosses represent the experimental data.

$\Gamma_7 \rightarrow \Gamma_7$ transitions would have different PDI curves when higher-order terms are taken into account, because of the presence of the α_0^0 term. For Nd^{3+} ions in $NdVO_4$, however, α_0^0 vanishes due to the negligibly small J mixing in the states of the ground multiplet and the PDI curves will be unchanged when higher-order terms are included. The relative magnitude of third-order spin-orbit to second-order contributions is numerically

TABLE X. Comparison between calculated and observed relative electronic Raman transition intensities in the $^4I_{9/2}$ ground multiplet of Nd^{3+} in $NdVO_4$ for the case $\tau = 0.48$. Estimated maximum uncertainties for the intensity measurements are about 20%. (-) indicates not observed.

Transitions (cm^{-1})		*ZZ* polarized		*XY* polarized		*XZ* polarized		*ZY* polarized	
Cal.[a]	Exp.	Cal.	Obs.	Cal.	Obs.	Cal.	Obs.	Cal.	Obs.
107	101	1.0	1.0	7.6	7.5	3.0	2.5	3.0	2.6
175	169	0	0	0.015	0	10	7.5	11.2	7.9
219	178	0	0	0	0	3.8	4.5	1.9	2.2
427	-	0	-	0.48	-	0.60	-	0.50	-

[a]From Ref. 25, see Table II.

TABLE XI. Relative magnitudes of the α_q^t parameters for the electronic Raman transition in $NdVO_4$ at 101 cm^{-1}. The calculated values include both the third-order spin-orbit and second-order contributions.

Transition 101 cm^{-1}	$((\alpha_0^1)/(\alpha_1^1))^2$	$((\alpha_1^1)/(\alpha_0^2))^2$	$((\alpha_0^1)/(\alpha_0^2))^2$
Fitted	0.73	7.4	10.2
Calculated (total)	0.78	6.28	8.05

$$(\alpha_0^0)^{3\mathrm{rd}}=0.0,$$

$$\frac{(\alpha_2^2)^{3\mathrm{rd}}}{(\alpha_2^2)^{2\mathrm{nd}}}=\frac{(\alpha_1^2)^{3\mathrm{rd}}}{(\alpha_1^2)^{2\mathrm{nd}}}=\frac{(\alpha_0^2)^{3\mathrm{rd}}}{(\alpha_0^2)^{2\mathrm{nd}}}=\frac{\langle {}^9I_{9/2}\|(\alpha^2)^{3\mathrm{rd}}\|{}^9I_{9/2}\rangle}{\langle {}^9I_{9/2}\|(\alpha^2)^{2\mathrm{nd}}\|{}^9I_{9/2}\rangle}=0.036,$$

and

$$\frac{(\alpha_1^1)^{3\mathrm{rd}}}{(\alpha_1^1)^{2\mathrm{nd}}}=\frac{(\alpha_0^1)^{3\mathrm{rd}}}{(\alpha_0^1)^{2\mathrm{nd}}}=\frac{\langle {}^9I_{9/2}\|(\alpha^1)^{3\mathrm{rd}}\|{}^9I_{9/2}\rangle}{\langle {}^9I_{9/2}\|(\alpha^1)^{2\mathrm{nd}}\|{}^9I_{9/2}\rangle}=0.0395$$

for all transitions in the ${}^4I_{9/2}$ ground multiplet of the Nd^{3+} ion in $NdVO_4$.

VI. CONCLUSION

We have reported PDI measurements for the phonon modes and electronic Raman transitions in the ground multiplets of Pr^{3+} and Nd^{3+} ions in vanadate crystals. The agreement between the relative intensities predicted by the second-order theory and those measured experimentally was very good. The third-order spin-orbit contribution was found to be approximately an order of magnitude less than the second-order contributions in both cases and therefore did not affect the results obtained from second-order calculations. The best fitted values of τ for $PrVO_4$ and $NdVO_4$ were 1.0 and 0.48, respectively. These values were in contrast with the considerably smaller fitted values for τ in Er^{3+}:YPO_4 and Tm^{3+}:YPO_4 reported by Becker *et al.*[6,7] The near unity values of τ in the case of Pr^{3+} and Nd^{3+} ions in vanadate crystals have confirmed the validity of Axe's theory when only the *d* configuration is included in calculating the ERS intensities.

The use of the PDI technique has proved to be important in determining the symmetries and origins of the ERS spectral lines. The PDI theory[20] predicted the intensities of one of the electronic Raman transitions in $PrVO_4$, whose line strength was sufficiently strong for accurate intensity measurements. The factor of 2 difference between the observed value of τ and the value of τ predicted by theory may be due to a lack of accurate wave functions for the ground multiplet of $PrVO_4$. There was excellent agreement between theory and experiment for $NdVO_4$.

ACKNOWLEDGMENTS

This research was sponsored by the Director, Office of Energy Research, Office of Basic Energy Sciences, Chemical Sciences Division of the U.S. Department of Energy under Contract No. De-AC03-76SF00098, and by the Division of Material Sciences, U.S. Department of Energy under Contract No. DE-AC05-84OR21400 with Martin Marietta Energy Systems, Inc.

[1] J. T. Hougen and S. Singh, Phys. Rev. Lett. **10**, 406 (1963).
[2] J. D. Axe, Phys. Rev. **136A**, 42 (1964).
[3] J. A. Koningstein and O. Mortensen, Phys. Rev. **168**, 75 (1968).
[4] J. A. Koningstein and O. Mortensen, J. Opt. Soc. Am. **58**, 1208 (1968).
[5] R. J. H. Clark and T. T. Dines, in *Advances in Infrared and Raman Spectroscopy*, edited by R. J. H. Clark and R. E. Hester (Heyden, London, 1982), Vol. 9, p. 282.
[6] P. C. Becker, N. Edelstein, G. M. Williams, J. J. Bucher, R. E. Russo, J. A. Koningstein, L. A. Boatner, and M. M. Abraham, Phys. Rev. B **31**, 8102 (1985).
[7] P. C. Becker, Ph.D. thesis, University of California, Berkeley, 1986.
[8] G. M. Williams, P. C. Becker, J. G. Conway, N. Edelstein, L. A. Boatner, and M. M. Abraham, Phys. Rev. B **40**, 4132 (1989).
[9] M. C. Downer, A. Bivas, and N. Bloembergen, Opt. Commun. **41**, 335 (1982).
[10] M. C. Downer and A. Bivas, Phys. Rev. B **28**, 3677 (1983).
[11] B. R. Judd and D. R. Pooler, J. Phys. C **15**, 591 (1982).
[12] B. Jacquier, Y. Salem, C. Linarès, J. C. Gâcon, R. Mahiou, and R. L. Cone, J. Lumin. , **38**, 258 (1987).
[13] M. C. Downer, C. D. Cordero-Monatalvo, and H. Crosswhite, Phys. Rev. B **28**, 4931 (1983).
[14] L. Smentek-Mielczarek, Phys. Rev. B **46**, 14 467 (1992).
[15] J. A. Koningstein and O. Mortensen, Nature (London) **217**, 45 (1968).
[16] O. Mortensen and J. A. Koningstein, J. Chem. Phys. **48**, 3971 (1968).
[17] We have used Koningstein and Mortensen's notation, in which the letters in the subscript represent the polarizations of the scattered and incident light reading from left to right.
[18] L. Smentek-Mielczarek, J. Chem. Phys. **94**, 5369 (1991); Phys. Rev. B **40**, 6499 (1989); **40**, 2019 (1989); **46**, 14 460 (1992); **46**, 14 453 (1992).
[19] A. D. Nguyen, Ph.D. thesis, University of California, 1996.
[20] A. D. Nguyen, Phys. Rev. B **55**, 5786 (1997).
[21] T. R. Bader and A. Gold, Phys. Rev. **171**, 997 (1968).
[22] B. Chakoumakos, M. M. Abraham, and L. A. Boatner, J. Solid State Chem. **109**, 197 (1994).
[23] P. Dawson, M. M. Hargreave, and G. R. Wilkinson, J. Phys. C **4**, 240 (1971).
[24] R. R. Andronenko, S. I. Andronenko, and A. N. Bazhan, Phys. Solid State **36**, 1302 (1994).
[25] P. Tanner and N. Edelstein, Chem. Phys. Lett. **152**, 140 (1988).
[26] B. Bleaney, R. T. Harley, J. F. Ryan, M. R. Wells, and M. C. K. Wiltshire, J. Phys. C **11**, 3059 (1978).
[27] P. C. Becker, N. Edelstein, B. R. Judd, R. C. Leavitt, and G. M. S. Lister, J. Phys. C **18**, L1063 (1985).
[28] T. Hayhurst, G. Shalimoff, J. G. Conway, N. Edelstein, L. A. Boatner, and M. M. Abraham, J. Chem. Phys. **76**, 3960 (1982).